Nucleation of Multiple Buckled Structures in Intertwined DNA Double Helices Supplementary Material

Sumitabha Brahmachari, Kathryn H. Gunn, Rebecca D. Giuntoli, Alfonso Mondragón, and John F. Marko
Department of Physics and Astronomy, and Department of Molecular Biosciences, Northwestern University, Evanston, Illinois 60208, USA

THEORY

In this section, we present a brief version of the detailed theoretical work done in Ref. [1]. We consider DNA braids made up of two torsionally unconstrained DNAs of length L under an applied force f, featuring a force-coupled straight braid state of length L_s and a plectonemically buckled state of length L_p. We also consider coexistence of m domains of the plectoneme state, where each domain is associated with a teardrop-shaped braid loop of size Γ. The total catenation number (Ca) is partitioned between the straight (Ca_s) and the plectonemically buckled region (Ca_p).

$$L = L_s + L_p + m\Gamma, \qquad \mathrm{Ca} = \mathrm{Ca}_s + \mathrm{Ca}_p. \tag{S1}$$

In the following, we present free energy expressions for the straight and the buckled states, which are then numerically minimized subject to the above constraints (Eq. S1), and compared with experiments (Figure S1).

The straight braid region consists of a helical section of length L_b and two end regions of total length $L_e \equiv L_s - L_b$. The end regions connect the helical section with the tethering points that are d apart on either ends [1]. The total mean-field energy of the straight braid (with radius R_s and pitch $2\pi P_s$ for the helical section, such that $L_b = 2\pi \mathrm{Ca}_s \sqrt{R_s^2 + P_s^2}$):

$$\beta\mathcal{E}_s = \frac{L_b A R_s^2}{(R_s^2+P_s^2)^2} - \beta f\left(L_b\cos\delta_s + L_e\cos\phi\right) + \frac{L_b}{A}\mathcal{U}_0(R_s,P_s), \tag{S2}$$

where the first term is the elastic bending energy of the helical section of the braid. The second term is the total force-extension energy, where $\delta_s \equiv \tan^{-1}(R_s/P_s)$ is the braiding angle, and $\phi \equiv \sin^{-1}(d/L_e)$ is the half of the opening angle in the end regions [1]. The third term is the Debye-Hückel electrostatic potential in the straight braid. R_s and P_s are determined from constrained minimization (Eq. S1) of the straight braid free energy.

We write the mean-field free energy of the plectoneme region composed of m domains [1]:

$$\begin{aligned}\beta\mathcal{E}_p = (L_p + m\Gamma)\left[\frac{A\sin^4\delta_p}{R_p^2} + \frac{1}{A}\mathcal{U}_0(R_p,P_p)\right] + L_p\left[\cos\delta_p\frac{A\sin^4\alpha}{4{R_p}^2} + \frac{2}{A}\mathcal{U}_0(\mathscr{R}_p,\mathscr{P}_p)\right] \\ + m\sqrt{2\varepsilon\beta A f} - \ln\left[\frac{(2\pi\mathrm{Ca}_s)^m(2\pi\mathrm{Tw}_p)^{m-1}}{m!(m-1)!}\right].\end{aligned} \tag{S3}$$

The first term (within brackets) corresponds to the bending and electrostatic energies of the braid in the plectoneme, where δ_p is the braiding angle in the plectoneme. The second term (within brackets) gives the elastic and electrostatic energies from the superhelical bending of the braid in the plectoneme, where $\mathscr{R}_p$ and $2\pi\mathscr{P}_p$ are respectively radius and pitch of the superhelical structure. The third and the fourth terms correspond to the total elastic energy and configuration entropy of m braid end loops respectively.

The total free energy contribution from worm-like-chain fluctuations[1]:

$$\begin{aligned}\beta\Delta\mathcal{F} = \frac{L_b}{A}\left[\frac{3}{2}\sqrt{\mu_s} + \eta_s^{1/4}\cos\left(\frac{1}{2}\tan^{-1}\sqrt{\frac{4\eta_s}{\mu_s^2}-1}\right)\right] + L_e\sqrt{\frac{2\beta f\cos\phi}{A}} \\ + \frac{(L_p+m\Gamma)}{A}\left[\frac{3}{2}\sqrt{\mu_p} + \eta_p^{1/4}\cos\left(\frac{1}{2}\tan^{-1}\sqrt{\frac{4\eta_p}{\mu_p^2}-1}\right)\right].\end{aligned} \tag{S4}$$

The first term (within brackets) corresponds to the helical section of the straight braid, whereas, the second term gives the fluctuation contribution from the two end regions. The third term corresponds to the braid in the plectoneme. μ_s and μ_p are the effective tension in each DNA in the braid of the straight and the plectoneme states respectively, whereas, η_s and η_p are the electrostatic moduli of radial deformations in the braid.

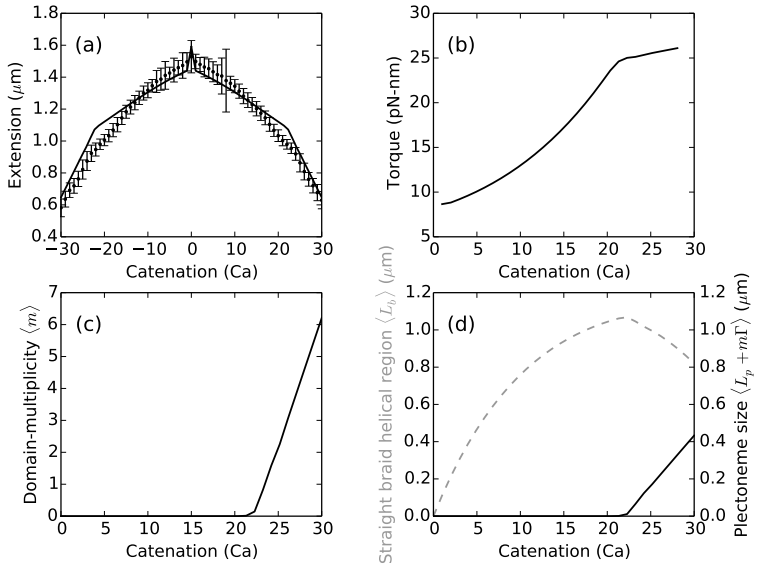

FIG. S1. Mechanical response of DNA braids made up of two torsionally unconstrained 6 kb DNAs ($L = 1.9$ μm) with intertether distance 0.74 μm ($d = 0.39L$) at 100 mM monovalent salt concentration, and under 1.5 pN force. (a) End-to-end extension of the braid z as a function of catenation Ca, where black points are experimental data at 1.5 pN. (b) Torque in the braid τ as a function of catenation shows a marked non-linear response before buckling. (c) Equilibrium number of plectoneme domains or domain-multiplicity m versus catenation number, showing appearance of multiple domains in the buckled state. (d) Length of the straight braid helical section L_b (gray dashed line) and the total size of the plectoneme region $L_p + m\Gamma$ (black solid line) versus catenation number. Increasing the catenation number in a braid builds up torque, which drives a buckling transition. Past the transition point, the buckled state grows featuring nucleation of new domains.

Now, the total free energy of the plectoneme coexistence state with given length of plectoneme L_p and domain-multiplicity m is obtained via numerical minimization of the total free energy over the straight phase catenation (Ca_s):

$$F(L_p, m) = \min_{\mathrm{Ca}_s} \left(\mathcal{E}_s + \mathcal{E}_p + \Delta\mathcal{F}\right). \tag{S5}$$

The above minimization (constrained by Eq. S1) ensures equilibrium. We sum over all possible coexistence states to construct a partition function:

$$\mathcal{Z}(\mathrm{Ca}, f) = e^{-\beta F(0,0)} + \sum_{m=1,2\ldots} \sum_{L_p} e^{-\beta F(L_p,m)}. \tag{S6}$$

The above partition function is then used to numerically calculate end-to-end extension z, average torque in the braid τ, pure-state variable $X \in \{R_s, P_s, \mathrm{Ca}_s\}$ and coexistence-state variable $Y \in \{\alpha, \delta_p, L_p, m\}$, as follows:

$$\langle z\rangle = -\frac{1}{\mathcal{Z}}\left[\frac{\partial F(0,0)}{\partial f} e^{-\beta F(0,0)} + \sum_{L_p,m} \frac{\partial F(L_p,m)}{\partial f} e^{-\beta F(L_p,m)}\right], \qquad \langle \beta\tau\rangle = -\frac{1}{2\pi}\frac{\partial \ln \mathcal{Z}}{\partial \mathrm{Ca}},$$
$$\langle X\rangle = \frac{1}{\mathcal{Z}}\left[X e^{-\beta F(0,0)} + \sum_{L_p,m} X\ e^{-\beta F(L_p,m)}\right], \qquad \langle Y\rangle = \frac{1}{\mathcal{Z}} \sum_{L_p,m} Y\ e^{-\beta F(L_p,m)}. \tag{S7}$$

The results of the numerical minimization are summarized in Figure S1.

EXPERIMENTS

As described before, the 6 kb DNA molecules used in braiding were made using one digoxigenin and one biotin 5′-labeled oligonucleotide as primers for PCR [2, 3]. The purified labeled DNA was diluted to 1 ng/μL in phosphate

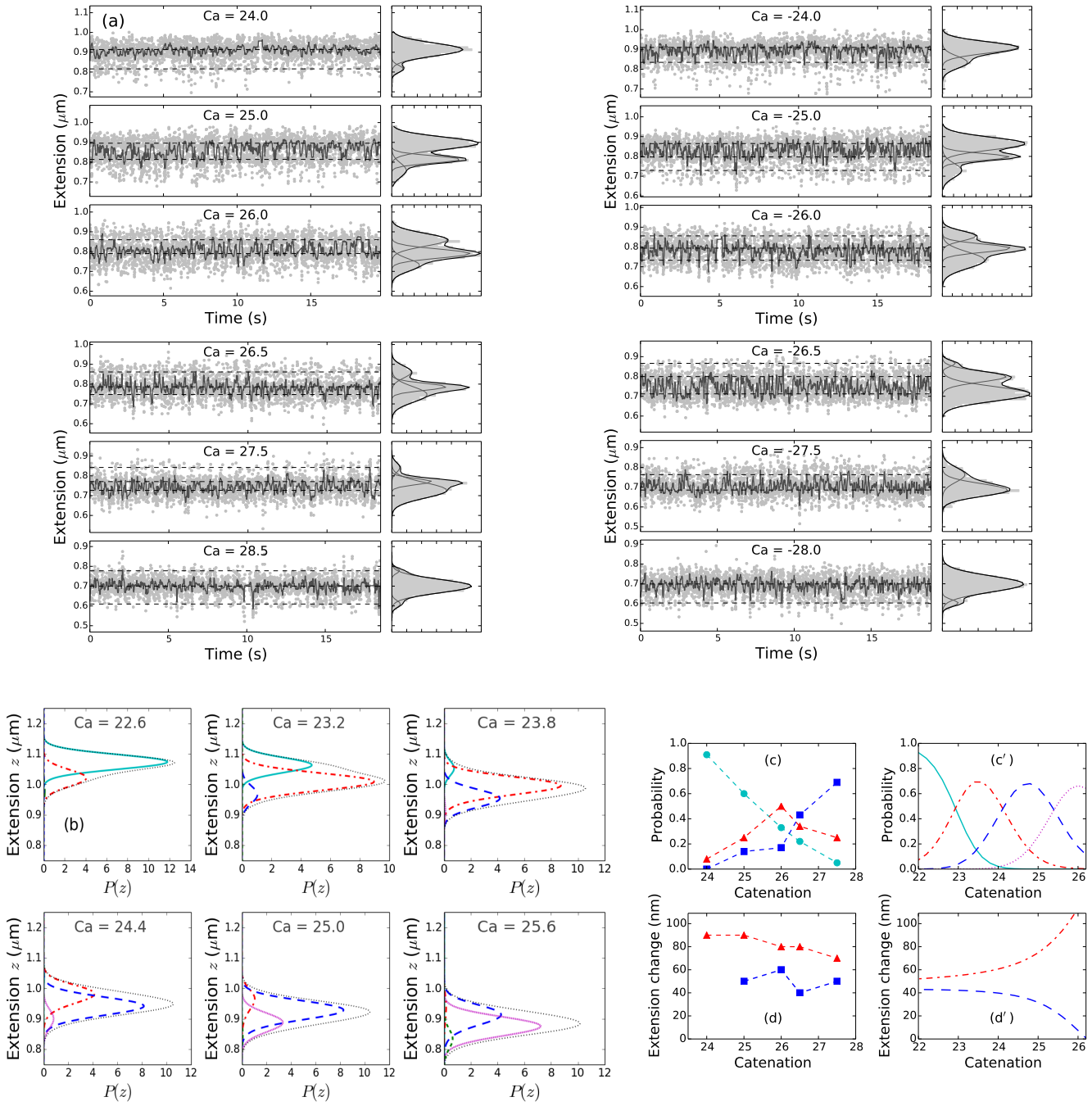

FIG. S2. (color online) Experiments and theory for 6 kb DNA braids ($L = 1.9$ μm) with intertether distance 0.74 μm ($d = 0.39L$), under 1.5 pN force at 100 mM NaCl (Figure S1). (a) Time-series data for braid extension near the buckling transition. Gray dots are raw experimental data taken at 200 Hz, which is then median filtered using a 0.1 sec time window to show dynamic switching (dark points). The adjacent right hand panels show histogram of the raw data (using 10 nm bins); the y-axis is the same left and right panels. The histograms were fit to a sum of three-parameter Gaussian distributions shown in black solid lines. The dashed line in the time series plot corresponds to mean of the individual best-fit Gaussians plotted on the right panels. (b) Theoretically predicted extension distributions (Eq. 4 of the main text) near the buckling transition point. The contributions from the straight braid (cyan solid lines) and the plectonemic braid composed of one (red dot-dashed lines), two (blue long-dashed line), three (magenta dotted lines) and four domains (green short-dashed lines) are plotted along with their sum shown in black dotted lines. (c) Probability of occupancy of the highest (cyan circles), the second highest (red triangles) and the third highest (blue squares) extension states, calculated from the area under the curve of the histograms. (c′) Theoretically predicted probability of the straight braid (cyan solid line) and the plectoneme braid with one (red dot-dashed line), two (blue dashed line) and three (magenta dotted line) domains. (d) Experimentally determined change in extension upon nucleation of the first (red circles) and the second (blue squares) buckled domain as a function of catenation. (d′) Theoretically predicted extension jump due to nucleation of the first (red dot-dashed line) and the second (blue dashed line) buckled domain as a function of catenation.

buffered saline (PBS) (17-516Q, Lonza) and incubated with 1 μm streptavidin coated paramagnetic beads (Dynabeads MyOne Streptavidin T1, 65601, Invitrogen) diluted to 0.6 mg/mL in 0.4 mg/mL Bovine Serum Albumin (BSA) (A7030 10G, Sigma-Aldrich). For the incubation, 1 μL of DNA was incubated with 2 μL of beads for 10 min. The beads and DNA were then diluted with 45 μL of PBS and passed into the flow cell [4]. Following a 20 min incubation in the flow cell, the slide was placed on the microscope and magnetic force applied. The bright-field magnetic tweezer microscope used for these experiments has been described before as part of Ref. [4]. To wash the DNA into the experimental buffer (100 mM NaCl, 20mM Tris-HCl pH 8), at least 6 flow cell volumes were passed through the flow cell. Following the identification of a potential DNA tether, the magnets were rotated to introduce turns (catenations) into the DNA. Single tethers would not supercoil, since the DNA only had single attachments to both the bead and glass coverslip, so only double tethers showed a change in extension with magnet rotation. After a double tether was identified, a lookup table was collected to measure the extension of the tethered bead compared to a fixed surface bead [5]. After exactly centering the double tether using the peak of the extension versus catenation curve as a guide, a force calibration was done using the Brownian motion of the bead [3, 6]. This calibration was used to estimate the force applied to the bead for the experiments. Data were collected at 200 Hz using a CMOS camera (PL-B741U, PixeLink), while the magnets were rotated to introduce or remove catenations in the braid.

[1] S. Brahmachari and J. F. Marko, Phys. Rev. E **95**, 52401 (2017).
[2] H. Bai, M. Sun, P. Ghosh, G. F. Hatfull, N. D. F. Grindley, and J. F. Marko, Proc. Natl. Acad. Sci. USA **108**, 7419 (2011).
[3] K. Terekhova, J. F. Marko, and A. Mondragón, Nucleic Acids Res. **42**, 11657 (2014).
[4] K. H. Gunn, J. F. Marko, and A. Mondragón, Nat. Struct. Mol. Bio. **24**, 484 (2017).
[5] C. Gosse and V. Croquette, Biophys. J. **82**, 3314 (2002).
[6] D. Skoko, B. Wong, R. C. Johnson, and J. F. Marko, Biomechistry **43**, 13867 (2004).